C h a p t e r 2

MOLECULAR DYNAMICS STUDY OF A BINARY CU-ZR METALLIC GLASS: GLASS FORMATION AND ATOMIC-LEVEL STRCTURE

We fitted the effective Rosato-Guillope-legrand (RGL)-type force field parameters for the binary Cu-Zr alloy system, carried out MD simulations for a Cu-Zr binary alloy, and studied the glass transition and the atomic-level structure of this system. An effective tight-bonding RGL-type n-body force field for the binary Cu-Zr alloy system was constructed and employed in MD simulations. Partial radial distribution functions, coordination numbers, and Honeycutt Andersen (HA) indices have been calculated to analyze the local structures of $Cu_{46}Zr_{54}$ metallic glass.

2.1. Introduction

Due to their high glass-forming ability, good processing ability, and exceptional stability

* Part of this chapter is reproduced from *Molecular Dynamic Study of the Binary $Cu_{46}Zr_{54}$ Metallic Glass Motivated by Experiments: Glass formation and Atomic-level structure*, by G. Duan, D.H. Xu, Q. Zhang, G.Y. Zhang, T. Cagin, W.L. Johnson, and W.A. Goddard III, *Physical Review B, 71, 224208 (2005), and Physical Review B, 74, 019901 (2006)*. Copyright 2005 and 2006 American Physical Society.

with respect to crystallization along with many promising properties such as high strength, elastic strain limit, fatigue resistance and corrosion resistance, bulk metallic glasses (BMGs) have acquired considerable attention from scientific as well as technological viewpoints in the last two decades [1-9]. As yet, researchers have developed families of multi-component systems to be BMG-forming alloys: Pd-, La-, Zr, Mg-, Y-, Ca-, Fe-, Ni-, and Cu-based, and have devoted a large amount of research work trying to obtain basic understandings of these glass-forming alloys [1-4, 10-18]. Very recently several binary BMGs have been identified in Ca-Al, Cu-Zr, and Cu-Hf alloy systems [12, 19-23] by the traditional copper mold casting method, which makes simple binary systems no longer a forbidden area when forming bulk amorphous alloys. The discovery of bulk- glass formers in binary systems, from an engineering point of view, can provide important guidance to the search for exceptional glass-forming alloys, and can improve the current alloy-developing efficiency significantly [18]. Also, simple binary systems might open new avenues towards the understanding of fundamental theoretical problems of BMG family alloys.

Molecular dynamics (MD) simulations have been successfully performed to analyze the structural, thermodynamic, and dynamic properties, and to investigate the glass forming mechanism of simple Cu-Y, Ni-Zr, Cu-Ag, Cu-Ni, Ni-Mo, Be-Zr, Ni-Zr-Al, Cu-W, Fe-C (B, P), and Cu-Mg amorphous alloys [24-40] at a microscopic level, on a scale ranging from the vibration to the mesoscopic times. However, most of these simple binary alloys mentioned above, which showed good glass-forming abilities in simulation processes, can not be fabricated into bulk amorphous samples experimentally. In this work, to develop a

better understanding of the glass formation and to investigate the relationship between properties and liquid structures in metal alloys, we employed MD simulation in conjunction with the quantum Rosato-Guillope-Legrand (RGL)-type many-body force field [41-42] to examine a Cu-Zr binary glassy alloy. The Cu-Zr model system was particularly chosen because we have discovered that the simple $Cu_{46}Zr_{54}$ alloy could be successfully cast into 2 mm fully amorphous strips by the copper mold casting method. In addition, for many excellent bulk-glass-forming alloys, such as Vitreloy 1 ($Zr_{41.2}Ti_{13.8}Cu_{12.5}Ni_{10}Be_{22.5}$) and Vitreloy 4 ($Zr_{47}$-$Ti_8Cu_{7.5}Ni_{10}Be_{27.5}$), if we take the Zr and Ti atoms simply as Zr, and Cu, Ni, and Be atoms simply as Cu, the alloy composition would be $Cu_{45}Zr_{55}$, which is very close to the binary bulk-glass former in composition in this work. Therefore, the present alloy $Cu_{46}Zr_{54}$ can play an important role as a model to probe the relationship between the properties and inherent structures for amorphous glassy alloys. Motivated by experimental progress, we fitted the effective RGL-type force field parameters for the binary Cu-Zr alloy system, and used MD simulation to study the glass transition and local structures of this simple metallic glass. It is extremely important to create appropriate interatomic potentials, generate glassy configurations, and study the local structures of the system before we can touch the next step.

In Section 2.2, we summarize various details of the calculations of the RGL-type many-body force field used to describe the Cu-Zr binary alloy system, and the MD approaches used in this work. Section 2.3 gives the results and discussions obtained from the simulations.

2.2. MD Simulation Details

2.2.1. Force Field and Parameters

The total energy of the system in Rosato-Guillope-Legrand (RGL)-type many-body force field (FF) [41-42] we used in the work has the following form.

$$U_{tot} = \sum_i U_i = \sum_i \left[E_B^i + E_R^i \right]$$

$$E_B^i = -\{ \sum_{i \neq j} c^2 Exp[-2q \, (\frac{r_{ij}}{r_0} - 1)] \}^{1/2}$$

$$E_R^i = \sum_{i \neq j} \frac{1}{2} \varepsilon Exp \, [-p \, \, (\frac{r_{ij}}{r_0} - 1)]$$

In these expressions, E_B and E_R denote the many-body metallic bonding potential and the pair-wise repulsive energy terms, respectively. r_0 is the first-neighbor distance in the AB lattice and the other four free parameters c,ε, p, q need to be fitted.

We first carried out Density Functional Theory (DFT) Quantum Mechanics (QM) calculations on various stable and unstable phases (SeqQuest program [43] was used): pure Cu, Pure Zr, CuZr(B2), Cu_2Zr_2 (Layered fcc), CuZr (B1), Cu_3Zr (fcc) and $CuZr_3$ (fcc). The QM results have shown to be in a good agreement with the experimental data [44]. The important physical properties were derived from QM and subsequently used as a reference to obtain the force field parameters. We fitted the force field parameters to the QM

calculated data such as lattice constants, cohesive energies, and bulk moduli. The obtained force field parameters are shown in Table 2.1 for Zr-Zr, Cu-Cu, and Cu-Zr. The comparisons between the FF results and the QM results for each phase of Zr, Cu and Cu-Zr are made in Tables 2.2 ~ 2.4, respectively. As we expect, the RGL-type force field describes Cu-Zr alloys quite well, and is suitable for studying Cu-Zr binary metallic glasses using MD simulation. From the RGL-type potential expressions, we notice that the atomic interactions decay exponentially with the increase of atomic spacing. Hence, it is applicable to set the cutoff distance as short as to include only two shells of atoms. In this work, we take the cutoff distance as 4.5 Å.

2.2.2. Molecular Dynamics

The simulations in this work are based on the constant-temperature, constant-thermo-dynamic-tension (TtN) MD method [45]. This method combines the Nose canonical ensemble [46] with the Parrinello-Rahman variable-shape-size ensemble [47, 48], and can capture very detailed microscopic information about the system, allowing us to study the phase transformation while permitting the shape and size of the cell to change. We can obtain data on volume, structure, and energy comparable to experimental data with an accurate force field.

We started our MD simulations from a super cell box with 2000 atoms (composition $Cu_{46}Zr_{54}$) under periodic boundary conditions. To generate the exact composition, we randomly substituted 80 copper atoms with the same amount of zirconium atoms in the B2 structure ($Cu_{50}Zr_{50}$ with 2000 atoms). The TtN MD simulations were carried out in a series

of increasing temperatures from 0 to 2400 K (a temperature several hundred degrees higher than the melting point) in 100 K increments. At each temperature the MD simulation time step was taken as 1 fs (10^{-15} seconds) and the simulation time for determining the properties was 20 ps (10^{-12} seconds). After equilibrating the structure in the liquid phase, we cooled the system using three different quenching rates (2.5, 5, and 10 K/ps) from 2400 K down to 100 K in 100 K decrements in the TtN ensemble. To achieve the set cooling rate, we kept the model system at the same temperature for times of 40, 20, and 10 ps, respectively.

Table 2.1. Rosato-Guillope-legrand (RGL)-type force field parameters.

	r_0 [Å]	ε	c	q	p
Zr-Zr	3.2100	0.3688	2.3365	2.0250	7.9273
Cu-Cu	2.6356	0.2149	1.3483	2.7490	10.2215
Cu-Zr	2.9086	0.3615	2.0100	2.7960	8.6020

Table 2.2. A comparison between RGL-type force field and QM results for Zr.

Phase	E_ff [eV/atom]	E_qm [eV/atom]	ΔE [%]	Ω_ff [Å^3]	Ω_qm [Å^3]	ΔΩ [%]
FCC	-6.21	-6.21	0.00	23.56	23.56	0.00
HCP	-6.21	-6.25	0.64	23.56	23.22	1.46
BCC	-6.04	-6.17	2.11	23.95	23.30	2.79
A15	-6.02	-6.10	1.31	24.18	23.33	3.64
SC	-5.75	-5.29	8.70	26.14	24.65	6.04
DM	-4.85	-3.56	36.24	34.84	32.01	8.84

Table 2.3. A comparison between RGL-type force field and QM results for Cu.

Phase	E_ff [eV/atom]	E_qm [eV/atom]	ΔE [%]	Ω_ff [Å^3]	Ω_qm [Å^3]	ΔΩ [%]
FCC	-3.49	-3.49	0.00	12.90	12.94	0.31
HCP	-3.49	-3.44	1.45	12.69	12.76	0.55
BCC	-3.42	-3.48	1.72	13.07	13.01	0.46
A15	-3.36	-3.38	0.59	13.35	13.32	0.23
SC	-3.09	-3.03	1.98	15.20	14.50	4.83
DM	-2.58	-2.45	5.31	21.58	20.84	3.55

Table 2.4. A comparison between RGL-type force field and QM results for Cu-Zr system.

Phase	E_ff [eV/atom]	E_qm [eV/atom]	ΔE [%]	Ω_ff [Å^3]	Ω_qm [Å^3]	ΔΩ [%]
CuZr (B2)	-4.98	-5.03	0.99	17.81	17.85	0.22
Cu_2Zr_2 (Layered FCC)	-5.01	-4.96	1.01	17.74	17.71	0.17
CuZr (B1)	-4.90	-4.65	5.38	19.68	19.69	0.05
Cu_3Zr (FCC)	-4.42	-4.11	7.54	15.17	15.83	4.17
$CuZr_3$ (FCC)	-5.57	-5.56	0.18	20.58	20.31	1.33

2.3. Results and Discussions

2.3.1. Glass Transition

Figure 2.1 presents the variation of volume as a function of temperature during the heating and cooling cycles. There is a noticeable jump in volume beginning at about 1400 K for the heating process, signifying the melting of the model. We can also observe the overlap stage between the heating and cooling curves, which indicates that our simulation system was melted. The reasons that we have a higher melting temperature than the equilibrium value might be the homogeneous model system without a free surface and the high heating rate.

From the cooling curve, we observe that there is a continuous change in volume compared to the heating process and no dramatic drop in the volume upon cooling. However, the slope of the volume vs. temperature curve decreases below 700 K, which is a sign of glass formation. As is well known, the glass transition is not a true thermodynamic 2^{nd}-order phase transition, since T_g is not fixed but depends on experimental conditions, particularly the cooling rate. At around the glass-transition temperature, changes in volume, enthalpy, and entropy are continuous and have a change in slope at T_g; however, their derivatives, such as heat capacity and thermal expansion coefficient, are discontinuous. We also investigated the effect of different cooling rates on the glass-transition temperature. Figure 2.2 shows the volume vs. temperature curves at three different quenching rates, 2.5 K/ps, 5 K/ps, and 10 K/ps, which reveals the cooling-rate dependence of glass-transition temperature. The faster cooling rate results in shorter times for the atoms to relax, thus

leading to a higher glass-transition temperature. In the present work we can observe a similar trend; however there is only a slight difference among the glass-transition temperatures.

A parameter often used as the measure of the phase transition (to glass or crystal) is the Wendt-Abraham parameter [49] extracted from the radial distribution function, which is defined by $R^{WA}=g_{min}/g_{max}$. Here g_{min} and g_{max} are the values of the radial distribution function $g(r)$ at the first minimum and the first maximum. The Wendt-Abraham parameter stresses the local character of $g(r)$, permitting a direct comparison between structures and leading to a sensitive estimation of glass-transition temperatures. We notice from our calculation that the temperature dependence of the Wendt-Abraham parameter R^{WA} leads to a clear intersection between two straight lines at $T_g = 700$ K, which is consistent with the intersection obtained from the volume vs. temperature curve.

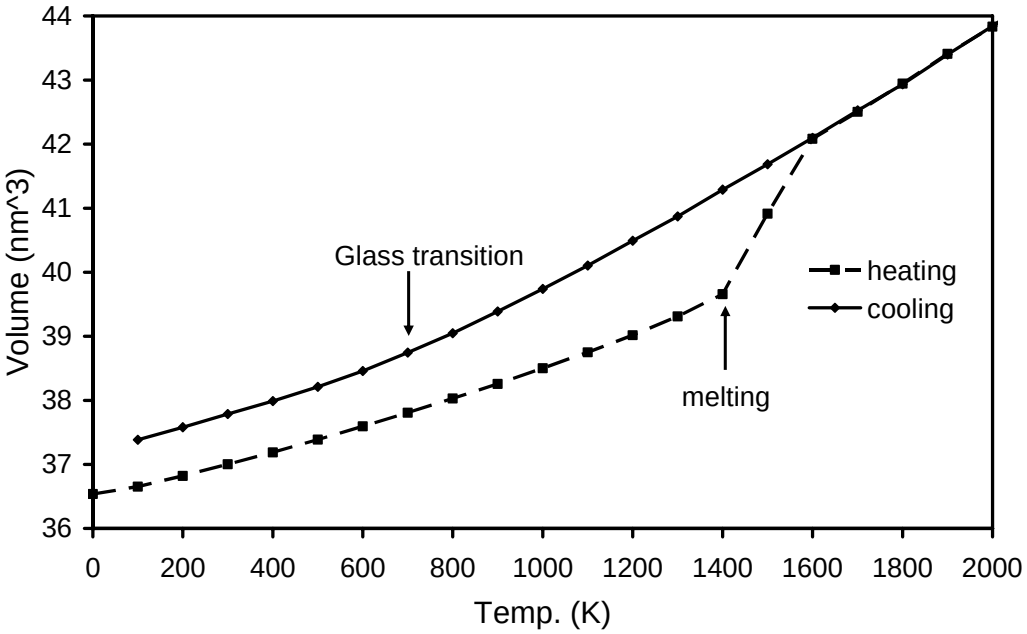

Figure 2.1. Volume as a function of temperature of $Cu_{46}Zr_{54}$ during heating and cooling at a rate of 5 K/ps.

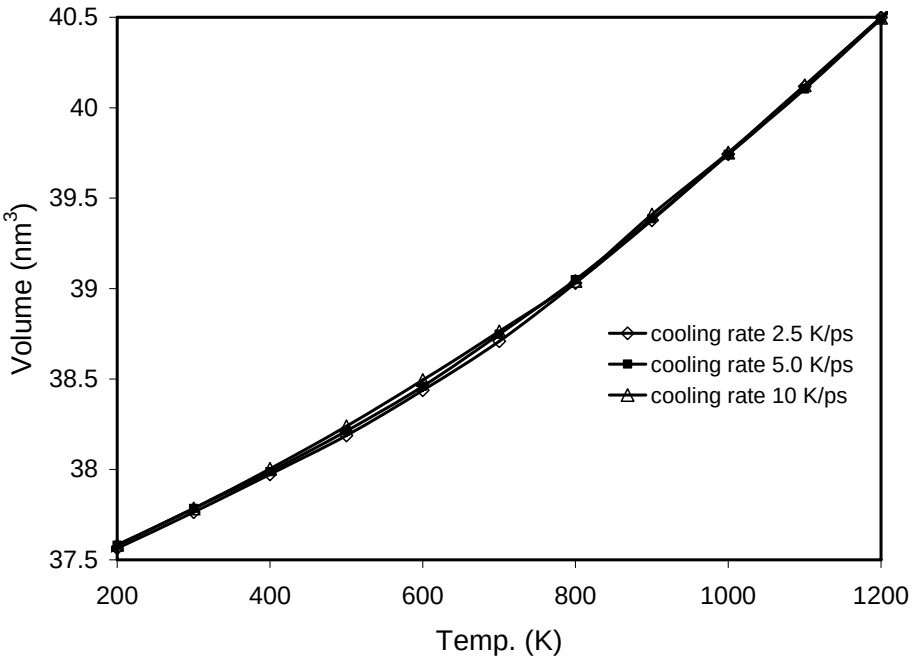

Figure 2.2. Volume vs. temperature curves for $Cu_{46}Zr_{54}$ obtained from three different quenching rates.

2.3.2. Radial Distribution Function

Radial distribution function (RDF) analysis is among one of the most important methods for revealing the structure features of a system, particularly for liquids and amorphous structures. The RDF can be calculated as:

$$g(r) = \frac{V}{N^2} \langle \sum_{i=1}^{n} \frac{n(r)}{4\pi r^2 \Delta r} \rangle$$

where N denotes the number of atoms in the simulation cell, V is the volume of the same cell, and n(r) is the number of particles which can be found in the shell from r to r + Δr. For the binary alloy system in this work, partial radial distribution function (PRDF) for atom α and atom β is calculated by

$$g_{\alpha\beta}(r) = \frac{V}{N_\alpha N_\beta} \langle \sum_{i=1}^{N_\alpha} \frac{n_{i\beta}(r)}{4\pi r^2 \Delta r} \rangle .$$

Figures 2.3, 2.4, and 2.5 present the PRDF of the model structure at different temperatures (400 K heating, 2000 K liquid state, and 400 K cooling) during the heating and cooling processes, respectively. We started our simulation from the random B2 structure, which can be seen clearly from the PRDF at 400 K in Figure 2.3. It shows the typical peaks of a B2 structure at σ, 1.16σ, 1.67σ, 1.96σ, and 2σ, where σ is the first nearest neighbor distance. Also we can observe from the PRDF that the first nearest neighbor positions are occupied by unlike atoms only, and the second nearest neighbor positions are occupied by like atoms only. However, at 2000 K the emergence of broad peaks in the PRDF (Figure 2.4) shows that the structure has melted and is in liquid state. For instance,

$g(r)_{Cu\text{-}Cu}$ indicates a peak at the first nearest neighbor distance 2.6 Å, which is close to the value of the liquid state of the pure element. Upon cooling to 400 K at the rate of 5 K/ps, we can also see that the feature of long-range disorder in the PRDF (Figure 2.5) and the second peaks of $g(r)_{Cu\text{-}Zr}$, $g(r)_{Cu\text{-}Cu,}$ and $g(r)_{Zr\text{-}Zr}$ are distinctly split as well, showing the formation of an amorphous phase [50]. The first peak of unlike pairs is relatively sharp compared with those of like atom pairs, which qualitatively suggests a preferred interaction of unlike atom pairs in this alloy. According to our calculations, the second peak splittings show up at $1.8\sigma_1$ and $2.08\sigma_1$ for Cu-Zr pair, at $1.75\sigma_2$ and $2.03\sigma_2$ for Cu-Cu pair, and $1.64\sigma_3$ and $1.95\sigma_3$ for Zr-Zr pair, respectively, where $\sigma_{1,}$ $\sigma_{2,}$ and σ_3 are the first peak positions. Thus quenching the $Cu_{46}Zr_{54}$ alloy from the liquid to 100 K at the rate of 5 K/ps leads to the formation of a metallic glass. We also examined the PRDF for the other two different cooling rates used in this work and similar PRDF distributions have been obtained.

As we have mentioned above, we can detect distinct splittings of the second peaks in all three PRDFs. However, the splitting occurs at different temperatures for $g(r)_{Cu\text{-}Cu,}$ $g(r)_{Cu\text{-}Zr}$, and $g(r)_{Zr\text{-}Zr.}$ Figures 2.6, 2.7, and 2.8 display the PRDFs of Cu-Cu pair, Cu-Zr pair, and Zr-Zr pair at different temperatures during the cooling cycle. We notice that for Cu-Cu pair, the splitting is already well developed at T_g, and in fact it first occurs at about 900 K (Figure 2. 6), which is well above T_g. (The temperature T_{split} is determined somewhat by visual inspection of the PRDFs at different temperatures.) For Zr-Zr and Cu-Zr pairs, the splittings occur at lower temperatures, 800K and 700 K, respectively. This reveals that some substructures have formed in like-atom pairs before reaching the final glassy state.

The local structure of metallic glasses in the binary Cu-Zr system has been studied experimentally using X-ray diffraction and EXAFS techniques [51, 52]. In these papers, the glassy samples were prepared by melt quenching or levitation melting, which should achieve a cooling rate on the order of 10^6 K/s. Table 2.5 lists the first peak positions of PRDFs obtained from three different techniques, X-ray diffraction, EXAFS, and calculation at room temperature. Note that the data represents two remarkably different cooling rates, on the order of 10^6 K/s for XRD and EXAFS data and 10^{12} K/s for the present simulation work. Our model system in simulation has larger nearest neighbor distances than those obtained from experiments. According to the Cohen-Grest free volume theory [53], upon cooling a glass-forming material from the liquid state some excess quenched-in free volume will be trapped into the glassy state, the quantity of which depends on the cooling rate. The higher the cooling rate, the larger the free volume in the final glassy state and thus the larger the nearest neighbour distances in the atom pairs.

Table 2.5. First peak positions from different techniques for amorphous Cu-Zr alloys.

	R (Cu-Cu) [Å]	R (Cu-Zr) [Å]	R (Zr-Zr) [Å]
$Cu_{50}Zr_{50}$ (XRD) [51]	2.53	2.75	3.15
$Cu_{46}Zr_{54}$ (EXAFS) [52]	2.54	2.72	3.14
$Cu_{46}Zr_{54}$ (Present)	2.67	2.78	3.22

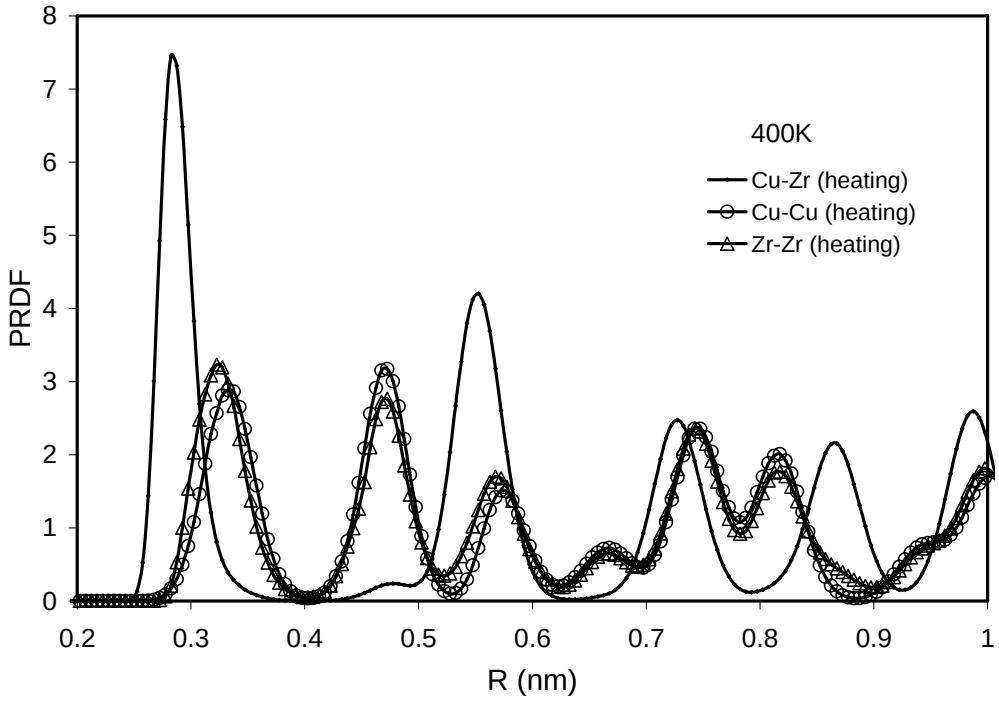

Figure 2.3. Partial radial distribution function (PRDF) of $Cu_{46}Zr_{54}$ for different bond pairs at 400 K during the heating process at the rate of 5 K/ps.

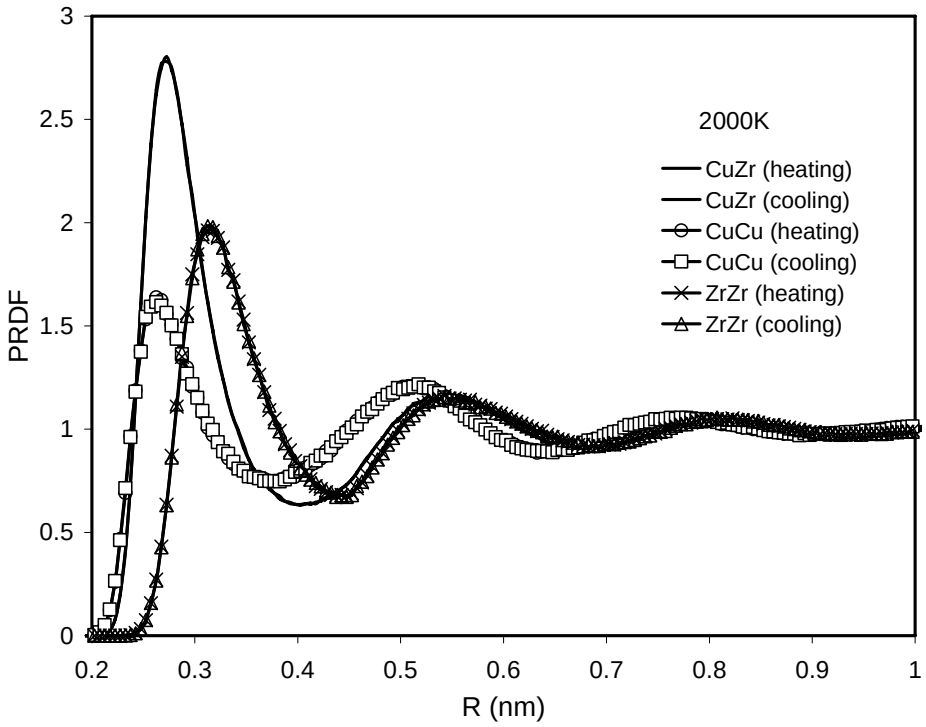

Figure 2.4. Partial radial distribution function (PRDF) of $Cu_{46}Zr_{54}$ for different bond pairs at 2000 K during the heating and cooling processes at the rate of 5 K/ps.

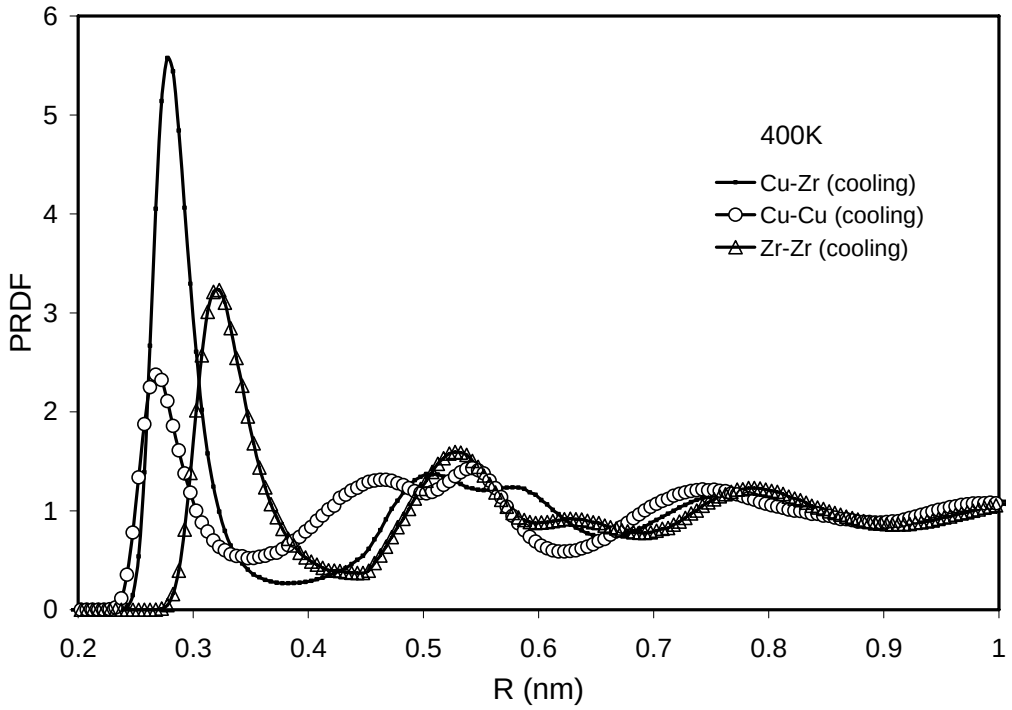

Figure 2.5. Partial radial distribution function (PRDF) of $Cu_{46}Zr_{54}$ for different bond pairs at 400 K during the cooling process at the rate of 5 K/ps.

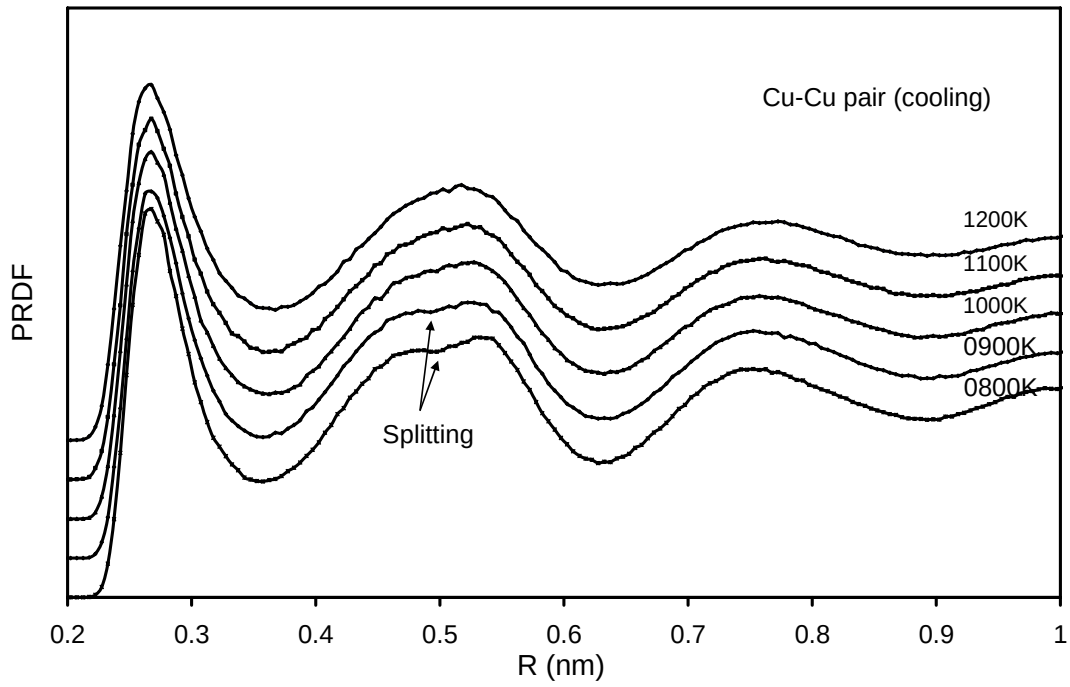

Figure 2.6. PRDF of $Cu_{46}Zr_{54}$ for different bond pairs during the cooling cycle at the rate of 5 K/ps, Cu-Cu pair.

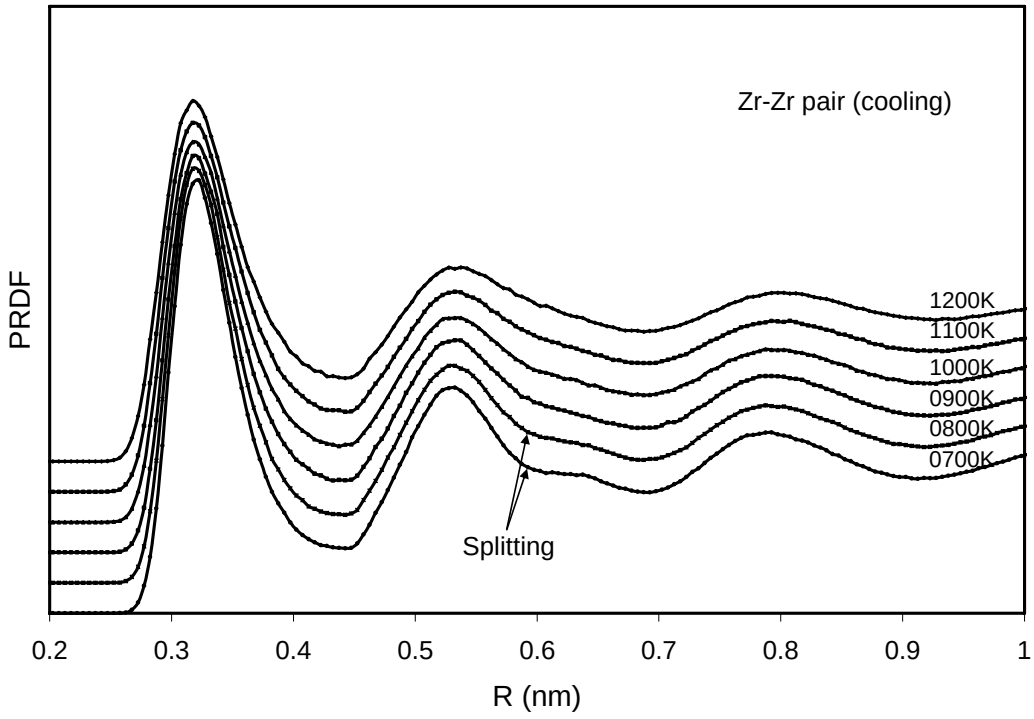

Figure 2.7. PRDF of $Cu_{46}Zr_{54}$ for different bond pairs during the cooling cycle at the rate of 5 K/ps, Zr-Zr pair.

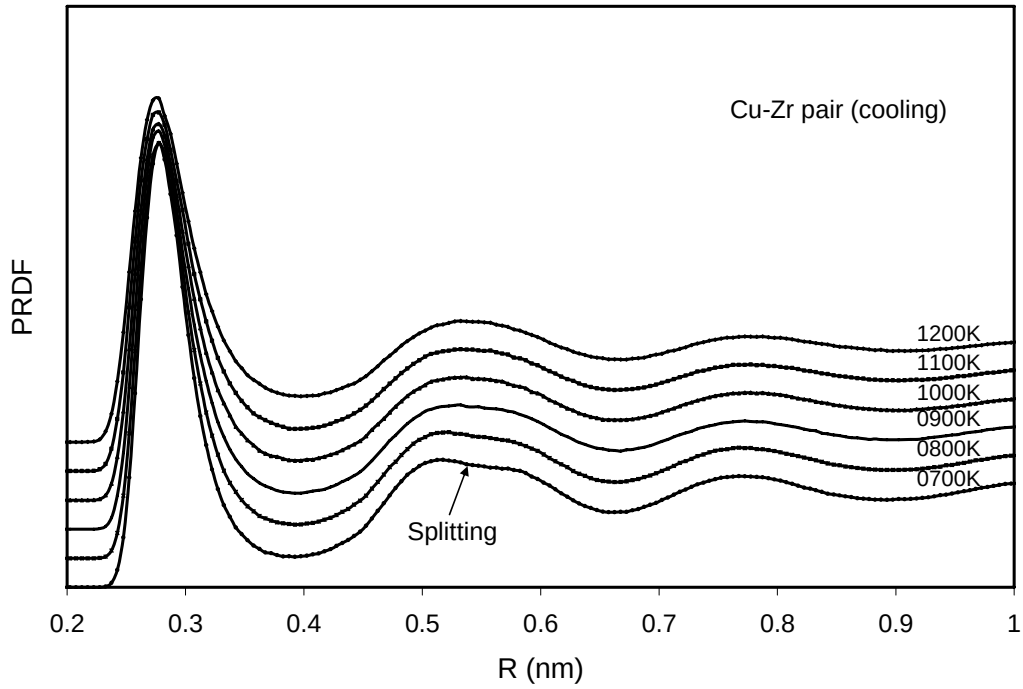

Figure 2.8. PRDF of $Cu_{46}Zr_{54}$ for different bond pairs during the cooling cycle at the rate of 5 K/ps, Cu-Zr pair.

2.3.3. Coordination Numbers

As is known, the coordination number is defined as the number of atoms bounded to a given atom in a structure. By integrating partial radial distribution function appropriately, we can determine the partial, total, and average coordination numbers, Z_{AB}, Z_A, and Z (the cutoff distance for the integration is taken as the first minimum point in PRDF). These are shown in Figure 2.9, for different temperature PRDFs from the cooling run. The average coordination number is quite independent of temperature change, Z=13.27±0.54. The coordination number of Zr is always higher than the average Z, and Z_{Cu} is always lower.

The numbers of nearest neighbor correlations extracted from three different techniques are listed in Table 2.6. We observe that the values indicate a more-or-less random distribution of metal atoms in amorphous Cu-Zr alloys, although a negative heat of mixing suggests the preferred atomic bonding of unlike atom pairs.

Table 2.6. The numbers of near-neighbour correlations obtained from different techniques.

	N (Cu-Cu)	N (Cu-Zr)	N (Zr-Cu)	N (Zr-Zr)
$Cu_{50}Zr_{50}$ (XRD) [51]	5.8	5.6	5.0	5.0
$Cu_{46}Zr_{54}$ (EXAFS) [52]	6.0	5.5	5.0	5.0
$Cu_{46}Zr_{54}$ (Present)	3.2	7.6	6.5	9.1

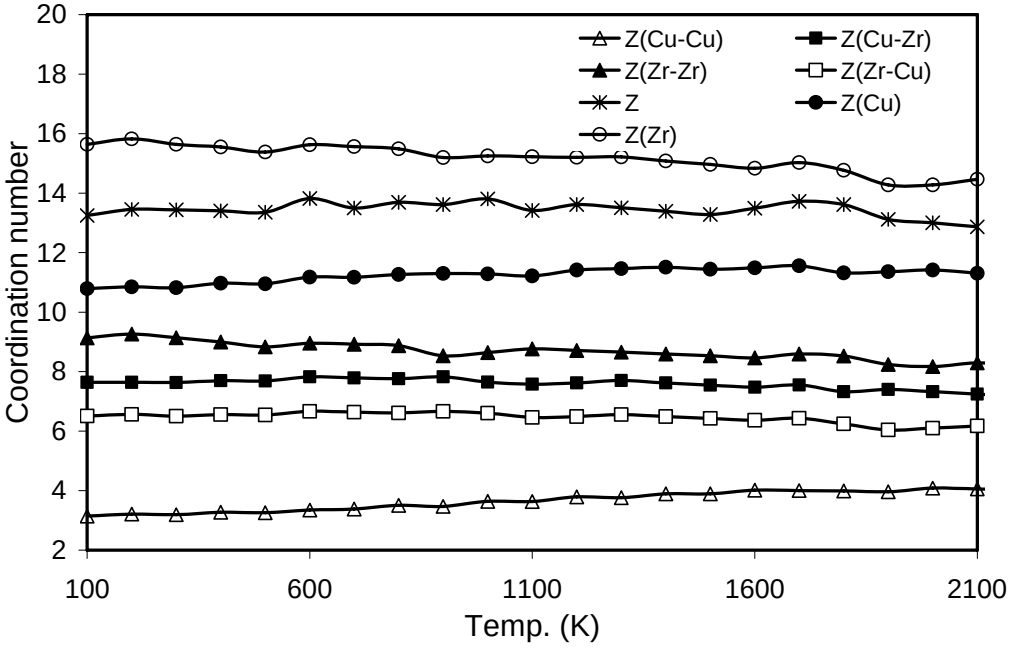

Figure 2.9. Partial, total, and average coordination numbers of $Cu_{46}Zr_{54}$ calculated for the cooling cycle with the rate of 5 K/ps.

2.3.4. Honeycut-Anderson Analysis

The absence of long-range order is the well-known characteristic of the atomic arrangement in amorphous structures. However, it is difficult to determine details of the atomic arrangement with the structure-probing techniques such as X-ray diffraction, due to the absence of long parallel rows and flat parallel planes of atoms in glasses. For such systems, Honeycutt-Andersen (HA) analysis has been proven to successfully assess local structures of amorphous phases [54-59, 37]. In this method, pairs of atoms are classified by: (i) whether or not they are near-neighbors; (ii) the number of near-neighbors they have in common; and (iii) the near-neighbor relationships among the shared neighbors. Therefore, a sequence of four integers (*ijkl*) is designed to characterize the local structure. The first integer i is to identify the bonding of two given atoms; i is 1 when they are bonded in the root pair, otherwise i is 2. The second integer j is the number of the near-neighbors shared in common by the two given atoms. The third integer k is the number of bonds among the shared neighbors. The fourth integer l is needed to differentiate between the cases when the first three indices are the same but the bond geometries are different. To determine whether or not two atoms are bonded, we use the first minimum in the PRDF for the particular pair of atoms at the temperature being calculated as the cutoff distance. Also the pair fractions of HA indices are normalized just for convenience, so that the sum over all cases for nearest neighbors (i = 1) adds up to unity.

Different structures have different HA indices and general observations are as follows: the face-centered cubic (FCC) structure leads only to 1421; the hexagonal close packed (HCP) structure leads to 50% 1421 and 50% 1422; the 13-atom icosahedron structure leads

to 71% 1321, 29% 1551, and also 71% 2331; while the binary bcc (B2) structure leads to 43% 1441 and 57% 1661, if A-A and B-B bonds are considered in addition to A-B bonds. In general, 1421 and 1422 are characteristics of the closest packed crystalline structures (FCC and HCP). 1441 and 1661 are characteristics of the B2 structure while 1551 and 2331 are characteristics of icosahedral ordering.

We first calculated the HA pair fractions for the beginning structure. The results show that this simulation cell leads to 42% 1441, 56% 1661 and fractions of 1551 pairs and 2331 pairs that are almost zero, which confirms our beginning random B2 structure. Upon heating to 1200 K before melting, the 1441- and 1661-pair fractions gradually decrease to 29% and 37%, respectively, although these two pairs are still the main components of the local structures. After melting at 2000 K, 1441 and 1661 drop to 7% and 6%, respectively while 1431, 1541, and 1551 increase to 16%, 12% and 14% respectively, showing the structure of a liquid state.

Figure 2.10 shows the HA pair fractions as a function of temperature when the binary $Cu_{46}Zr_{54}$ system was cooled down from 1500 K to 400 K. We can observe that in the cooling simulation the 1441 and 1661 pairs do not change much over the whole temperature range. The 1441 pair fraction changes from about 8% at 1500 K to 10% at 700 K (glass transition temperature), and then remains almost constant until 400 K. The 1661 pairs follow the behavior of 1441, reaching 8% at 1500 K supercooled liquid state, increasing to 14% at T_g, and being nearly unchanged until 400 K. In contrast, the icosahedral 1551 and 2331 pairs increase uniformly as the system supercools until local maxima of 92% of 2331 and 34% of 1551 are reached at 700 K, indicating that the final

state after quenching with a cooling rate of 5 K/ps is amorphous. Therefore, as the model system is cooled from its liquid state, the icosahedral symmetry keeps increasing until the model system reaches the phase transition point. Recently the short-range-order structures of amorphous solids have been characterized in kinds of metallic glasses by Neutron diffraction and EXAFS local environmental probing techniques [60-64]. Evidence of icosahedral short-range-order in $Zr_{70}Cu_{30}$ and $Zr_{70}Cu_{29}Pd_1$ has been reported [61], and it supports the theory claiming a correlation between the existence of local icosahedral short range order and the stability of the supercooled liquid state. It has also been shown that the icosahedral topological local order develops to a very high degree even in an amorphous Ni-Ag alloy, with no tendency to form quasicrystals [63]. The HA index analysis of $Cu_{46}Zr_{54}$ metallic glass in the present work is in good agreement with these experimental progress.

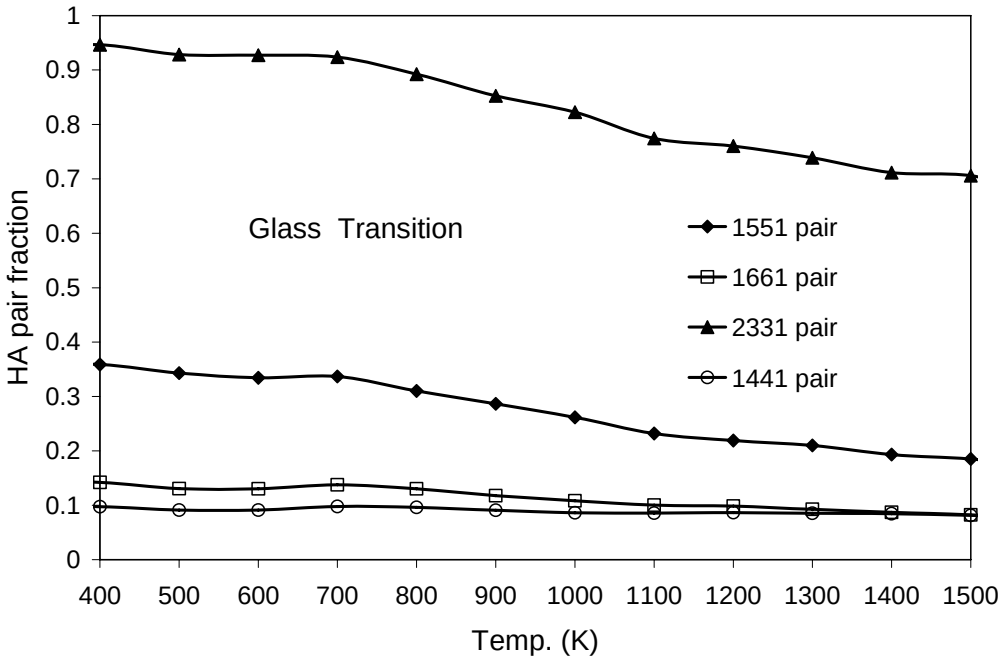

Figure 2.10.Variation of the fractions of Honeycutt-Andersen indices during the cooling cycle at the rate of 5 K/ps.

2.4. Chapter Concluding Remarks

An effective tight-bonding RGL-type n-body force field for the binary Cu-Zr alloy system was constructed and employed in MD simulations. Partial radial distribution functions, coordination numbers, and Honeycutt Andersen (HA) indices have been calculated to analyze the local structures of $Cu_{46}Zr_{54}$ metallic glass. Distinct splittings of the second peaks have been observed in all three Cu-Cu, Cu-Zr, and Zr-Zr PRDFs, and the splittings occur at different temperatures for different atom pairs. The higher cooling rate from the MD simulation results in larger free volume and accordingly larger nearest neighbor distances in the atom pairs compared with those obtained from experiments. HA-index analysis reveals a high degree of the local icosahedral five-fold short-range-order structure in the present MD glassy alloy.

References

[1] A.L. Drehman, A.L. Greer, D. Turnbull, Appl. Phys. Lett. 41, 716 (1982).

[2] A. Inoue, T. Zhang, T. Masumoto, Mater. Trans. JIM 31, 425 (1990).

[3] T. Zhang, A. Inoue, T. Masumoto, Mater. Trans. JIM 32, 1005 (1991).

[4] A. Peker, W.L. Johnson, Appl. Phys. Lett. 63, 2342 (1993).

[5] W.L. Johnson, Mater. Res. Soc. Bulletin 24, 42 (1999).

[6] A. Inoue, A. Takeuchi, Mater. Trans. 43, 1892 (2002).

[7] J. Basu, S. Ranganathan, Sadhana Acad. Proc. Eng. Sci. 28, 783 (2003).

[8] J.F. Löffler, Intermetallics 11, 529 (2003).

[9] W.H. Wang, C. Dong, C.H. Shek, Mater. Sci. & Eng. R 44, 45 (2004).

[10] A. Inoue, A. Kato, T. Zhang, S.G. Kim, T. Masumoto, Mater. Trans. 32, 609 (1991).

[11] F.Q. Guo, S.J. Poon, G.J. Shiflet, Appl. Phys. Lett. 83, 2575 (2003).

[12] F.Q. Guo, S.J. Poon, G.J. Shiflet, Appl. Phys. Lett. 84, 37 (2004).

[13] Z.P. Lu, C.T. Liu, J.R. Thompson, W.D. Porter, Phys. Rev. Lett. 93, 245503 (2004).

[14] V. Ponnambalam, S.J. Poon, G.J. Shiflet, J. Mater. Res. 19, 1320 (2004).

[15] V. Ponnambalam, S.J. Poon, G.J. Shiflet, J. Mater. Res. 19, 3046 (2004).

[16] H. Choi-Yim, D.H. Xu, W.L. Johnson, Appl. Phys. Lett. 82, 1030 (2003).

[17] D.H. Xu, G. Duan, W.L. Johnson, C. Garland, Acta Mater. 52, 3493 (2004).

[18] D.H. Xu, G. Duan, W.L. Johnson, Phys. Rev. Lett. 92, 245504 (2004).

[19] D. Wang, Y. Li, B.B. Sun, M.L. Sui, K. Lu, E. Ma, Appl. Phys. Lett. 84, 4029 (2004).

[20] D.H. Xu, B. Lohwongwatana, G. Duan, W.L. Johnson, C. Garland, Acta Mater. 52 2621 (2004).

[21] M.B. Tang, D.Q. Zhao, M.X. Pan, W.H. Wang, Chin. Phys. Lett. 21, 901 (2004).

[22] G. Duan, D.H. Xu, W.L. Johnson, Meta. Mater. Trans. A, 36A, 455 (2005).

[23] A. Inoue, W. Zhang, J.J. Saida, Mater. Trans. 45, 1153 (2004)

[24] R. Frattini, R.G. Dellavalle, Phys. Rev. B 50, 3620 (1994).

[25] H. Teichler, Phys. Rev. Lett. 76, 62 (1995).

[26] T. Aihara, Y. Kawazoe, T. Masumoto, J. Non-Cryst. Solids 207, 875 (1996).

[27] R.R. Nurgayanov, V.G. Chudinov, Glass Phys. Chem. 23, 400(1997).

[28] Y. Qi, T. Cagin, Y. Kimura, W.A. Goddard, Phys. Rev. B 59, 3527 (1999).

[29] Z.C. Li, B.X. Liu, Chin. Phys. Lett. 16, 667 (1999).

[30] M.I. Mendelev, S.N. Ishmaev, F. Hajdu, G. Meszaros, E. Svab, Mater. Sci. Forum 321, 496 (2000).

[31] H. Teichler, J. Non-Cryst. Solids 293, 339 (2001).

[32] M. Guerdane, H. Teichler, Phys. Rev. B 65, 014203 (2002).

[33] K. Brinkmann, H. Teichler, Phys. Rev. B 66, 184205 (2002).

[34] Y. Qi, T. Cagin, Y. Kimura, W.A. Goddard, J. Computer-Aided Materials Design 8 (2-3), 233 (2002).

[35] H.R. Gong, L.T. Kong, W.S. Lai, B.X. Liu, Phys. Rev. B 68, 144201 (2003).

[36] A.V. Evteev, A.T. Kosilov, E.V. Levtchenko, Acta Materialia 51, 2665 (2003).

[37] H.-J. Lee, T. Cagin, W.L. Johnson, W.A. Goddard, J. Chem. Phys. 119, 9858 (2003).

[38] N.P. Bailey, J. Schiotz, K.W. Jacobsen, Phys.Rev. B 69, 144205 (2004).

[39] M. Shimono, H. Onodera, Mater. Trans. 45, 1163 (2004).

[40] F. Albano, N. Lacevic, M.L. Falk, S.C. Glotzer , Mater. Sci. Eng. A 375-77, 671 Sp. Iss. (2004).

[41] V. Rosato, M. Guillope, B. Legrand, Philos. Mag. A 59, 321 (1989).

[42] F. Cleri, V. Rosato, Physical Review B 48, 22 (1993).

[43] P.A. Schultz, Sandia National Laboratories. (For more information, please check http: //www.cs.sandia.gov/~paschul/Quest/.)

[44] H. -J. Lee, Ph. D. thesis, California Institute of Technology, 2003.

[45] J.R. Ray, A. Rahman, J. Chem. Phys. 82, 4243 (1985).

[46] S. Nose, Mol. Phys. 52, 255 (1984); S. Nose, J. Chem. Phys. 81,511 (1984).

[47] M. Parrinello, A. Rahman, Phys. Rev. Lett. 45, 1196 (1980).

[48] M. Parrinello, A. Rahman, J. Appl. Phys. 52, 7182 (1981).

[49] H. R. Wendt and F. F. Abraham, Phys. Rev. Lett. 41, 1244 (1978).

[50] J. L. Finney, Nature (London) 266, 309 (1977).

[51] H.S. Chen, Y. Waseda, Phys. Stat. Sol. A 51, 593 (1979).

[52] A. Sadoc, Y. Calvayrac, A. Quivy, M. Harmelin, A.M. Flank, J. Non-Cryst. Solids 65, 109 (1984).

[53] M.H. Cohen, G.S. Grest, Phys. Rev. B 20, 1077 (1979).

[54] J. D. Honeycutt and H. C. Andersen, J. Phys. Chem. 91, 4950 (1987).

[55] H. Jonsson and H.C. Andersen, Phys. Rev. Lett. 60, 2295 (1988).

[56] D.W. Qi and S. Wang, Phys. Rev. B 44, 884 (1991).

[57] K. Chen, H. Liu and Z. Hu, J. Phys.: Condens. Matter 7, 517 (1995).

[58] H. Li, G. Wang, X. Bian and F. Ding, Phys. Rev. B 65, 035411 (2001).

[59] H. Li, G. Wang, J. Zhao, X. Bian, J. Chem. Phys. 116, 10809 (2002).

[60] T.C. Hufnagel, S. Brennan, Phys. Rev. B 67, 014203 (2003).

[61] K. Saksl, H. Franz, P. Jovari, K. Klementiev, E. Welter, A. Ehnes, J. Saida, A. Inoue, J.Z. Jiang, Appl. Phys. Lett. 83, 3924 (2003).

[62] A. Di Cicco, A. Trapananti, S. Faggioni, A. Filipponi, Phys. Rev. Lett. 91, 135505 (2003).

[63] W.K. Luo, H.W. Sheng, F. M. Alamgir, J.M. Bai, J.H. He and E. Ma, Phys. Rev. Lett. 92, 145502 (2004).

[64] K. Ahn, D. Louca, S.J. Poon, G.J. Shiflet, Phys. Rev. B 70, 224103 (2004).